Jinst

PUBLISHED BY IOP PUBLISHING FOR SISSA MEDIALAB

RECEIVED: *October 31, 2019*
REVISED: *February 27, 2020*
ACCEPTED: *March 9, 2020*
PUBLISHED: *April 23, 2020*

INTERNATIONAL SUMMER SCHOOL ON
INTELLIGENT SIGNAL PROCESSING FOR FRONTIER RESEARCH AND INDUSTRY
HUAZHONG UNIVERSITY OF SCIENCE AND TECHNOLOGY, HUST, AT WUHAN, CHINA
12–26 MAY 2019

2020 JINST 15 C04043

The mechanism of edge effect in CdZnTe pixel detector and an improved design of pixel sizes of anode

R. Wu,[a,1,2] M.J. Heng,[b,2] G.Q. Zha[a] and W.Q. Jie[a]

[a] *State Key Laboratory of Solidification Processing,*
MIIT Key Laboratory of Radiation Detection Materials and Devices,
School of Materials Science and Engineering, Northwestern Polytechnical University
Xi'an 710072, Shaanxi, People's Republic of China

[b] *Northwest Institute for Non-ferrous Metal Research,*
Xi'an 710072, Shaanxi, People's Republic of China

E-mail: wurui@mail.nwpu.edu.cn

ABSTRACT: In this paper, the mechanism of the edge effect in Cadmium Zinc Telluride (CZT) pixel detectors is studied, and the energy spectrum performance and the charge collection efficiency of peripheral pixels with reduced sizes are analysed by computer-aided simulation and measurement. The results show that the distribution of the weighting potential, which is determined by the electrode structure, has significant influence on the edge effect. Reducing the sizes of peripheral pixels can optimize the weighting potential and improve the detection performance. A detector with reduced peripheral pixel sizes is prepared. We build a gamma imaging system using this kind of detector, test the spectrum response to ^{137}Cs@662 keV and image a M10 nut under the collimated ^{241}Am@59.5 keV. The measured spectrum of the edge/corner/intermediate pixels is consistent with the simulated spectrum and the obtained countingtype gray-scale image of the nut clearly shows its shape and sizes. These results prove that reducing peripheral pixel sizes has practical value in gamma imaging technology.

KEYWORDS: Detector design and construction technologies and materials; Gamma detectors (scintillators, CZT, HPGe, HgI etc); Image reconstruction in medical imaging; Medical-image reconstruction methods and algorithms, computer-aided diagnosis

[1]Corresponding author.
[2]These authors contribute equally to this article.

https://doi.org/10.1088/1748-0221/15/04/C04043

Contents

1 Introduction

In recent years, Cadmium Zinc Telluride (CZT) detectors have been paid great attention because of their special features. CZT has a large average atomic number and a wide band gap, meaning it has high detection efficiency and can work at room temperature with stable chemical properties. The resistance of CZT is usually larger than 10^9 Ω·cm and its detectable energy range is from more than 20 keV to several MeV. Many international organizations have positioned CZT as a key material in the field of high energy detection at room temperature [1] and think of it as a substitute for scintillator detectors in the next decades. The typical values of mobility for electrons and holes in CZT are 1000–800 $\mathrm{cm^2V^{-1}s^{-1}}$ and 80–30 $\mathrm{cm^2V^{-1}s^{-1}}$ and the lifetime is $1–3 \times 10^{-6}$ s and $0.1–1 \times 10^{-6}$ s, respectively [2, 3]. It is obvious that the hole mobility-lifetime product is much smaller than that of the electron. Therefore, for further application and development of CZT detectors, a crucial challenge is to break through the restriction of the incomplete charge collection caused by low mobility-lifetime product of holes.

Large gamma imaging systems based on CZT pixel detectors have shown potential in many fields, such as nuclear radiation monitoring, nuclear medicine, safety inspection, space science, and nondestructive examination [4, 5]. These require higher requirements in detector performance than conventional scintillator detectors, such as larger area, higher efficiency, higher sensitivity and higher spatial resolution. However, there are still many problems to solve: (1) The influence of the edge effect on pixel detectors. The performance of a CZT pixel detector is limited by the crystal size, which is generally small and depends on crystal growth technology. To solve this problem, researchers have considered using a series of small CZT pixel detectors to mosaic a larger imaging system. Generally, the performance of edge pixels is worse than that of intermediate pixels, which is termed the edge effect. This is a common phenomenon in pixel detectors, which results in inhomogeneity of detection and limits the fabrication and development of large area CZT gamma imaging systems. (2) The signal crosstalk between pixels [6]. The electron-hole pairs are generated in CZT crystal under the irradiation of radiation. These charge clusters broaden their sizes during the drift procession and produce different degrees of charge sharing in adjacent pixels. (3) The limitation of detection efficiency. At present, the gamma imaging technique and

2020 JINST 15 C04043

image reconstruction are achieved by using mechanical collimators. Most of the incident γ-rays are absorbed by collimators. The proportion of rays actually detected makes up a very small part of the total quantity. This situation greatly weakens the detection efficiency of a gamma camera. Especially when used in medical treatments, the low detection efficiency could greatly increase the radiation dose borne by patients [7].

Keeping the problems that exist in gamma imaging systems in mind, this paper focuses on the improvement of the edge effect in CZT pixel detectors. First, the causes of the edge effect are analyzed. Second, a workable solution, reducing the size of the peripheral pixels, is simulated by computer simulation. Finally, a CZT pixel detector with reduced peripheral pixels is prepared. We then test the spectrum response to ^{137}Cs@662 keV and image a M10 nut by collimated ^{241}Am@59.5 keV to investigate the reliability of simulation results and imaging performance of the detector.

2 Analysis and experiment

2.1 The mechanism of edge effect

First, composition deviation and defect concentration are more likely to occur on the surface of the CZT crystal than in the crystal during the processing. These factors will increase the number of trapped carriers and result in incomplete charge collection and deterioration of energy resolution in edge pixels.

Second, there are fluctuations in the energy distribution of incident radiations and the interactions between γ-rays and CZT are also indefinite. In the intermediate area of the pixel detector, the ray is close to the normal incidence, while in the edge area, the direction of the ray incidence is an acute angle, so compared with the intermediate area, the interaction becomes more complicated in edge area. Further, there is a possibility that Compton scattering occurs, which produces recoil electrons and scattered photons at nearby pixels. Edge pixels are more affected because the path dispersion of photons that enter the crystal from these areas is larger. These factors result in statistical fluctuation of induced charge and complicate the signal crosstalk.

Finally, there is a difference in the distribution of weighting potential in different pixels and different positions of a pixel. Take the following detector as an example. We define the coordinate system as shown in the figure 1(a) to describe the detector. The origin of the coordinates is on the cathode plane directly below the upper left corner of the anode. The CZT detector is $10\times10\times5\,\mathrm{mm}^3$ in (x, y, z) with a pixelized anode at $z = 5$ mm and a plane cathode at $z = 0$ mm, other geometric details are illustrated in figure 1(a). The equipotential diagrams of the weighting potential of the intermediate and corner pixel marked with dots are shown in figure 1(b). The cross sections are marked as dash line in figure 1(a). It can be seen that the symmetry of equipotential distribution of intermediate pixel is better than that of corner pixel. The equipotential lines are densely distributed in intermediate pixel while for corner pixels, loosely. According to Shockley-Ramo theory [8, 9], in the case of the pixel detector, when two electrons are placed at any symmetrical position of an intermediate pixel and allowed to move to this pixel, they can produce the same amount of induced charge. Under the same assumptions for corner pixels, the amount of induced charge produced by electrons close to the center is larger than that of electrons close to surface of side edge. Therefore, the charge collection gets nonuniform because of the symmetry difference in corner and intermediate pixels. The edge effect of the pixel detector comes out.

2020 JINST 15 C04043

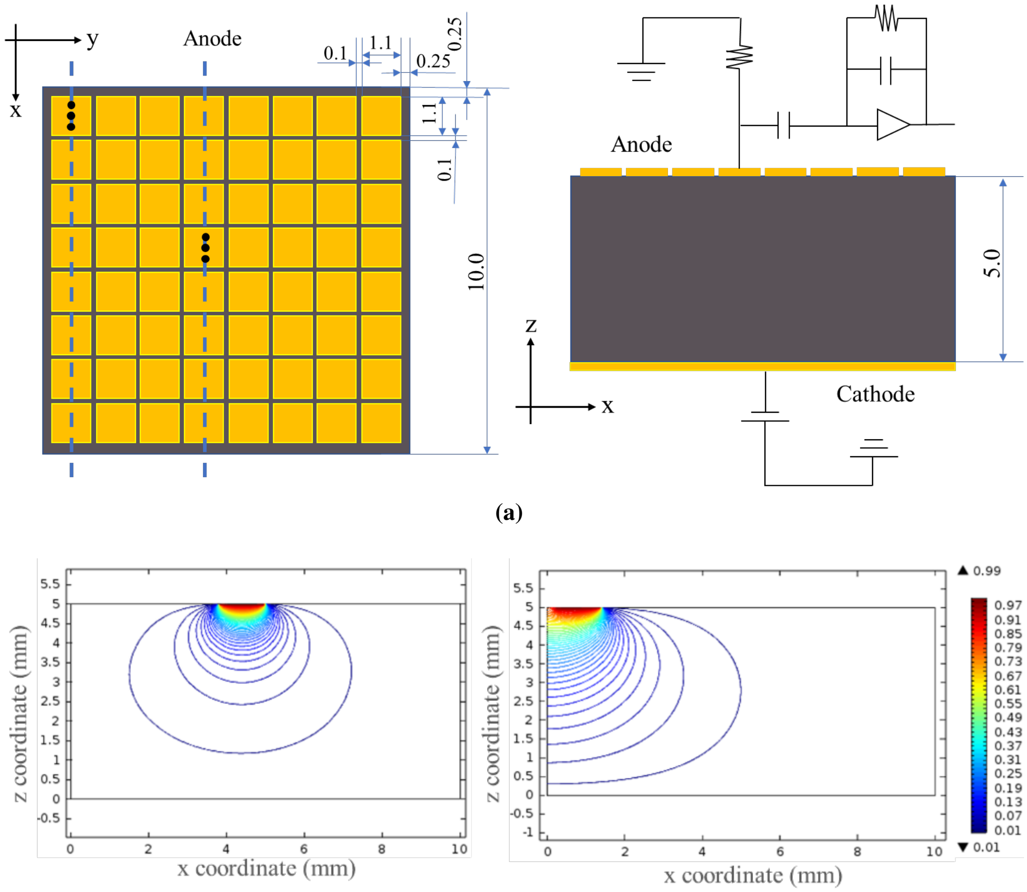

(a)

(b)

Figure 1. (a) A description of anode pixel and the cross-section, the cross sections of intermediate (5.4 mm in y) and corner pixels (0.8 mm in y) are illustrated as dash line. (b) Equipotential diagrams of the weighting potential of intermediate and corner pixels on given cross sections.

2.2 The improvement of edge effect

The 2D diagram of equipotential distribution mentioned above can describe the intrinsic property of the pixel detector clearly, but it doesn't seem to be an easy way to quantitatively study the characteristion of the weighting potential field and its effect on detection performance. So we simplify it and research a series of 1D weighting potential lines in specific positions of the equipotential distribution to simplify the processing and calculation.

In CZT, as mentioned above, the hole has low mobility-lifetime product, and it can be easily captured by crystal defects during the motion, resulting loss in induced charge. It is more practical to collect electrons at anode as electrons have much higher mobility-lifetime product. The pixelated anode structure can be optimized to tune the weighting potential distribution.

A weighting potential comparison of intermediate and corner pixel in the different positions is shown in figure 2. The positions are illustrated as black dots in figure 1(a). The weighting potential increases gradually from 0 to 1 from the cathode to the anode. For the intermeiate pixel, in most areas from cathode, the weighting potential is small and increases at a very slow rate. It rises

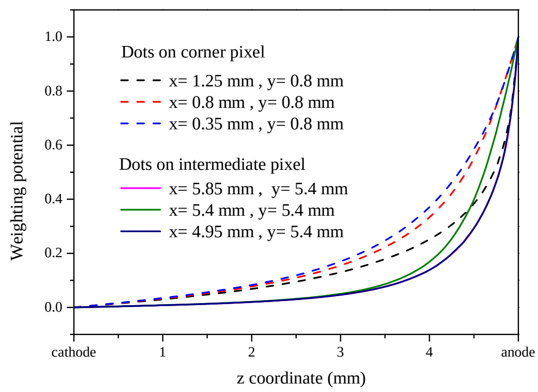

Figure 2. A comparison of weighting potential distributions in the different positions of intermediate pixel and corner pixel. These positions are illustrated as black dots in figure 1(a).

rapidly at around one-pixel length to the anode. For the corner pixel, the weighting potential has risen to a higher level at the same distance to the anode and incerases with a slower rising speed towards the anode than that of intermediate pixel. It's worth noting that the weighting potential of the two symmetrical positions (the y coordinate is 5.4 mm and the x coordinate is 5.85 mm and 5.4 mm, respectively) relative to the center of the intermediate pixel coincide. But for corner pixel, the weighting potential of the two symmetrical positions show different rising speeds. The weighting potential at $x = 0.35$ mm, $y = 0.8$ mm is larger than the weighting potential at $x = 1.25$, $y = 0.8$ mm in any position from cathode to anode.

The primary causes of the difference between the weighting potential curves are the difference in symmetry of the equipotential distribution on different pixels and the difference in the degree of denseness at different positions on a pixel. As shown in figure 1(b), the equipotential lines form ring-closures in intermediate pixels, while for corner pixels, the equipotential lines partially form ring-closures, and partially terminate outside the pixel or the side of the detector forming ring-openings. The equipotential distribution of intermediate pixel is dense. Therefore, the three weighting potential curves of the intermediate pixel rise faster near the anode and the uniformity of these curves is better.

A series of pixel detectors with different peripheral pixel sizes are fabricated by computer aided simulation. The coordinate system of these detectors is the same as the one defined in figure 1(a). 8×8 anode pixels are prepared on the top square ($z = 5$ mm) of a $10 \times 10 \times 5\,\mathrm{mm}^3$ in (x, y, z) CZT crystal and a $10 \times 10\,\mathrm{mm}^2$ plane cathode is prepared on the bottom square ($z = 0$ mm). The intermediate pixel size is $1.1 \times 1.1\,\mathrm{mm}^2$ in all detectors. The corner pixel length d ranges from 1.1 mm to 0.6 mm with a decrease of 0.1 mm at a time and the size is $d \times d\,\mathrm{mm}^2$. The edge pixel size is determined by its position which is either $1.1 \times d\,\mathrm{mm}^2$ or $d \times 1.1\,\mathrm{mm}^2$. The gaps between the pixels are 0.1 mm in all detectors. The energy spectrum response to ^{137}Cs@662 keV of corner pixels with different sizes is calculated. As shown in figure 3, as the corner pixel size reduces from $1.1 \times 1.1\,\mathrm{mm}^2$ to $0.6 \times 0.6\,\mathrm{mm}^2$, the shape of the full-energy peak becomes more and more similar to a gaussian peak. The symmetry increases and the broadening gets smaller, thus the energy resolution increases. The low-energy tailing reduces with the increase in the peak counts, this is because the total number of events remains the same in simulation.

2020 JINST 15 C04043

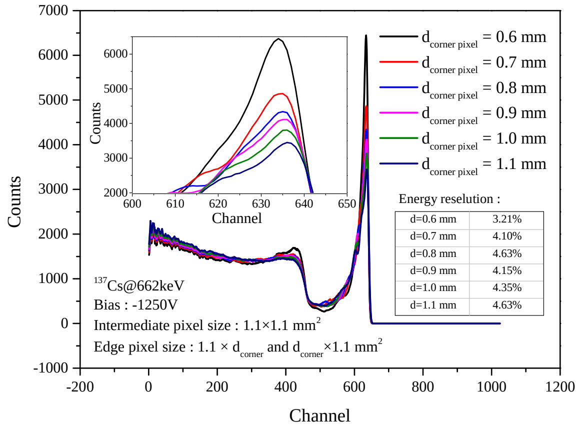

Figure 3. Spectrum of ^{137}Cs@662 keV with different corner size.

Figure 4(left) shows the comparison of weighting potential of corner pixels with different sizes and figure 4(right) shows the comparison of weighting potential of intermediate, edge and corner pixel before and after reducing the sizes. In figure 4, the weighting potential comes from the center point of the corresponding pixel. It is clear to see, as the size decreases, the weighting potential becomes uniform in a larger range and rises in a faster speed and a shorter distance when approaching the anode. The weighting potential of the intermediate pixel is not affected by the size of peripheral pixels. Decreasing the size of the corner and edge pixels can make the shape of the weighting potential in these positions close to that of the intermediate pixels which benefits to improve the uniformity of charge collection in different positions and optimize the detection performance. So a reasonable size design can improve the intrinsic properties of peripheral pixels to the level of intermediate pixels and achieve a more uniform detection performance. It's an effective method to reduce the edge effect.

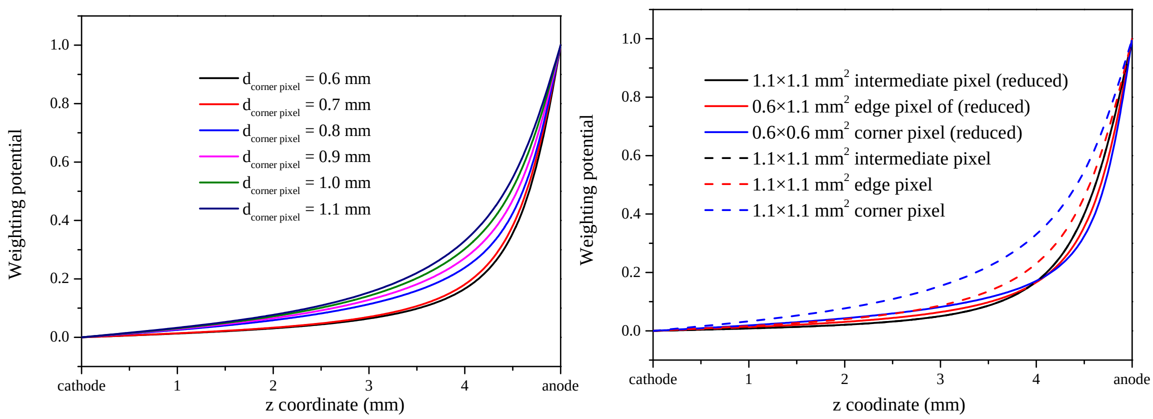

Figure 4. The weighting potential of corner pixels with different sizes (left) and the weighting potential of intermediate, edge and corner pixel before and after reducing the sizes (right). The weighting potential comes from the center point of the corresponding pixel.

The induced charge collection efficiency of different corner pixels is calculated in figure 5. At the cathode, the maximum charge collection efficiency appears here because of the contribution of

2020 JINST 15 C04043

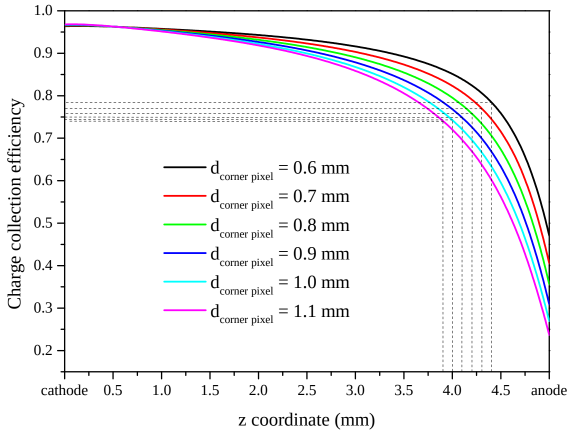

Figure 5. Charge collection efficiency of corner pixels with different sizes.

electrons that drift full path length. As z coordinate increases, the holes are gradually captured for the low mobility-lifetime product during the drift and this becomes the main factor that decreases the induced charge. It's obvious that as the pixel size decreases, the degree of charge collection loss decreases. At the anode, the charge collection efficiency of the corner pixels with the size of $0.6 \times 0.6\,\mathrm{mm}^2$ and $1.1 \times 1.1\,\mathrm{mm}^2$ is 0.47 and 0.24, respectively. The reason why the charge collection efficiency increases as the pixel size decreases is as follows: as mentioned above, the shape of the weighting potential of $0.6 \times 0.6\,\mathrm{mm}^2$ corner pixel and $0.6 \times 1.1\,\mathrm{mm}^2$ edge pixel are similar to that of the $1.1 \times 1.1\,\mathrm{mm}^2$ intermediate pixel, which means the amounts of induced charge generated on these pixels are at almost the same level of the intermediate pixel. This improvement decreases as the corner pixel size increases. In addition, the sharper the weighting potential rises near the anode, the larger the potential gradient here and the greater the induced charge generated by charge movement. At the same time, the hole is not easily captured because the velocity of the hole is large in the place where the potential gradient is large. So, the charge collection efficiency at anode increases as the pixel size decreases. Small peripheral pixels are conducive to achieve high and uniform charge collection.

To sum up, reducing the size of edge and corner pixels is a feasible method to achieve a better weighting potential distribution and improve the charge collection efficiency. It can reduce the full energy peak broadening of the spectrum and improve the energy resolution. It makes sense to improve detection uniformity of the CZT pixel detector.

2.3 Preparation and performance evaluation

First, the CZT crystal is cut a little larger than $25.4 \times 25.4 \times 5\,\mathrm{mm}^3$ in (x, y, z). Then the crystal's surface is polished with a magnesium oxide suspension as a first step and a mixture of silica gel and hydrogen peroxide as a second step. Next, the polished surface is etched with a bromine methanol to obtain a mirror-like surface. The final size of the obtained CZT crystal is $25.4 \times 25.4 \times 5\,\mathrm{mm}^3$. Finally, a pixel array of 16×16 is fabricated on one square plane by photoetching and vapor deposition, with a pixel sizes of $1.5 \times 1.5\,\mathrm{mm}^2$ in the intermediate pixels, $1.5 \times 1.35\,\mathrm{mm}^2$ or $1.35 \times 1.5\,\mathrm{mm}^2$ in the edge pixels, and $1.35 \times 1.35\,\mathrm{mm}^2$ in the corner pixels. The gap between the pixels is 0.1 mm. The pixel distribution on the anode is shown in figure 6 and the sizes of pixels

2020 JINST 15 C04043

and gaps are marked. A planar electrode is evaporated on the other square plane as the cathode, with a size of $25.2 \times 25.2\,\mathrm{mm}^2$. Gold is used as the electrode material for the detector.

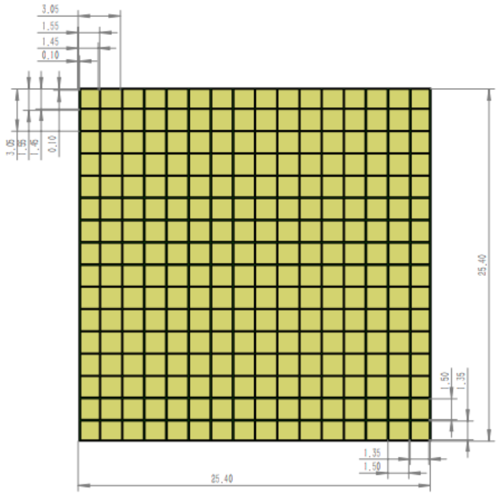

Figure 6. Diagram of anode pixels of CZT detector.

An infrared microscope is used to observe the inclusion in the crystal. The crystal's resistivity and leakage current are determined by an I-V test, and the energy spectrum response of the ^{241}Am@59.5 keV is tested without detector packaging. Experimental results show that there is no obvious grain boundary in the CZT crystal, the inclusion distribution is uniform, the resistivity is more than $10^9\,\Omega\cdot$cm, the working leakage current is less than 10 nA, and the energy resolution of ^{241}Am@59.5 keV is less than 7%.

The energy spectrum response to ^{137}Cs@662 keV is tested using the self-built gamma imaging system. After the low-energy noise is filtered out, the counts on different channels of each pixel are recorded. We extract the signals at the edge pixel, corner pixel, and intermediate pixel of the detector from the measured data to obtain the energy spectrum. At the same time, the energy spectrum under the same detector construction and working condition is simulated, the measured and simulated spectrums are shown in figure 7(left) and figure 7(right) respectivily. It's clear to see that the measurement and simulation reflect the same rules, the intermediate pixel has the best energy spectrum performance, followed by the edge pixel and the angle pixel. There are many factors that would affect the practical measurement, such as the existence of crystal defects, the unpredictable incidence direction of rays, the irregular statistical fluctuation caused by electronic noise, etc., which make the peak-to-compton ratio of the measured spectrum lower than that of the simulated one. But for the edge effect studied in this paper, the simulation results can clearly and intuitively reflect its influence.

The counting-type gray-scale image of a M10 nut under the collimated ^{241}Am@59.5 keV is obtained by calculating the peak counts of different pixels after filtering out the noise and deducting radioactive source. The radioactive source is collimated by a pixelated parallel-hole collimator. The collimator is a 5 mm thick alloy plate with 32×32 through-holes, the diameter of each through-hole is 1.3 mm. We place the detector under a quarter of the collimator and make sure one pixel corresponds to one through-hole of the collimator. The through-holes we actrally use is a 16×16 matrix. The nut

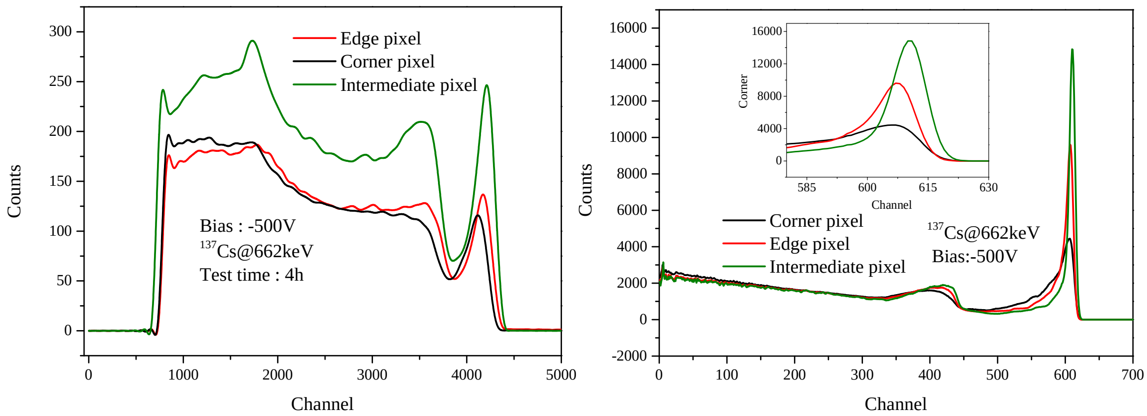

Figure 7. The measured (left) and simulated (right) energy spectrums of ^{137}Cs@662 keV of intermediate, edge and corner pixel under the bias of −500 V.

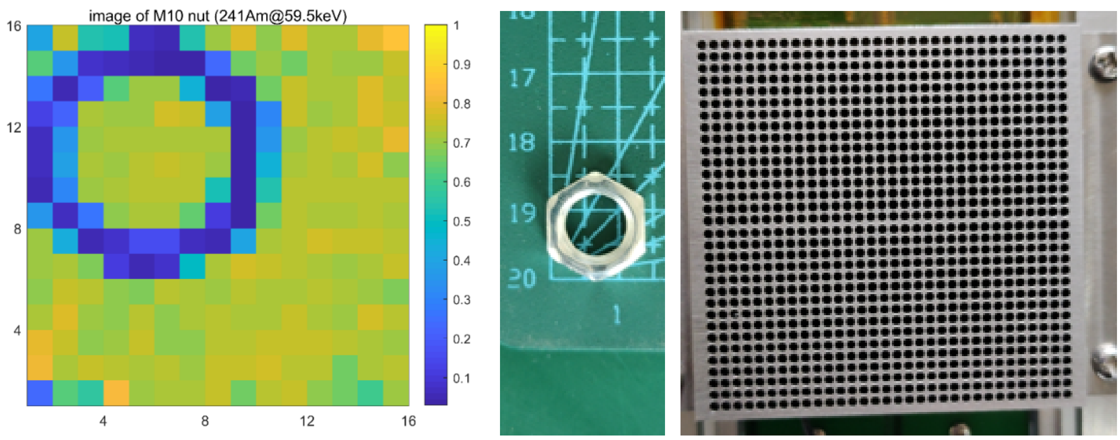

Figure 8. The counting-type gray-scale image of a M10 nut under the collimated ^{241}Am@59.5 keV (left) and the photos of the nut and collimator (right).

is placed on the upper left of the detector. By using the collimator, only the radiation that parallel to the through-holes can hit the CZT, the charge collection and energy spectrum response on the pixels can directly reflect the blocking effect of the nut on rays. Figure 8(left) is the rebuilt image of the M10 nut. The nut size inferred from the image basically matches the national standard, with only slight differences. We believe that this design is certainly valuable and there is also much work to do in the future. This improvement is expected to improve the current shortcomings in imaging technology and it's significant in field of nuclear radiation monitoring and nuclear medicine.

3 Conclusion

In this paper, the mechanism and the influence factors of the edge effect in CZT pixel detectors are analyzed and studied. The weighting potential plays a critical role in determining the pixel performance. Fabricating pixel detectors with normal intermediate pixels and reduced peripheral pixels has been proved to be a viable method to improve the edge effect of pixel detectors in this

2020 JINST 15 C04043

paper. This design is conducive to solving the problem of image distortion at the edge pixels in conventional pixel detecors, and will greatly promote the development and application of CZT pixel detectors in the field of gamma imaging.

Acknowledgments

This study has been financially supported by fund of MIIT(MJ-2017-F-05) and National Natural Science Foundation of China (61874089). The authors would like to give special thanks to Imdetek Ltd. for the great help during the experiment.

References

[1] R. Carchon, M. Moeslinger, L. Bourva, C. Bass and M. Zendel, *Gamma radiation detectors for safeguards applications*, *Nucl. Instrum. Meth.* **A 579** (2007) 380.

[2] C. Szeles, *Advances in the crystal growth and device fabrication technology of CdZnTe room temperature radiation detectors*, *IEEE Trans. Nucl. Sci.* **51** (2004) 1242.

[3] H. Chen, S.A. Awadalla, K. Iniewski, P.H. Lu, F. Harris, J. Mackenzie et al., *Characterization of large cadmium zinc telluride crystals grown by traveling heater method*, *J. Appl. Phys.* **103** (2008) 014903.

[4] B. Milbrath, A. Peurrung, M. Bliss and W. Weber, *Radiation detector materials: An overview*, *J. Mat. Res.* **23** (2008) 2561.

[5] T. Schlesinger, J. Toney, H. Yoon, E. Lee, B. Brunett, L. Franks et al., *Cadmium zinc telluride and its use as a nuclear radiation detector material*, *Mat. Sci. Eng.* **R 32** (2001) 103.

[6] J.C. Kim, S.E. Anderson, W. Kaye, F. Zhang, Y. Zhu, S.J. Kaye et al., *Charge sharing in common-grid pixelated CdZnTe detectors*, *Nucl. Instrum. Meth.* **A 654** (2011) 233.

[7] C.A. Raji and T.A. Henderson, *PET and single-photon emission computed tomography in brain concussion*, *Neuroimaging Clin.* **28** (2018) 67.

[8] W. Shockley, *Currents to conductors induced by a moving point charge*, *J. Appl. Phys.* **9** (1938) 635.

[9] S. Ramo, *Currents induced by electron motion*, *Proc. IRE* **27** (1939) 584.

2020 JINST 15 C04043